Nationaal Lucht- en Ruimtevaartlaboratorium

National Aerospace Laboratory NLR

NLR-TR-2014-019

Tonal generation by an airfoil at low to moderate Reynolds numbers

F. Gijsman

Nationaal Lucht- en Ruimtevaartlaboratorium
National Aerospace Laboratory NLR

Anthony Fokkerweg 2
P.O. Box 90502
1006 BM Amsterdam
The Netherlands
Telephone +31 (0)88 511 31 13
Fax +31 (0)88 511 32 10
www.nlr.nl

Nationaal Lucht- en Ruimtevaartlaboratorium
National Aerospace Laboratory NLR

Executive summary

Tonal generation by an airfoil at low to moderate Reynolds numbers

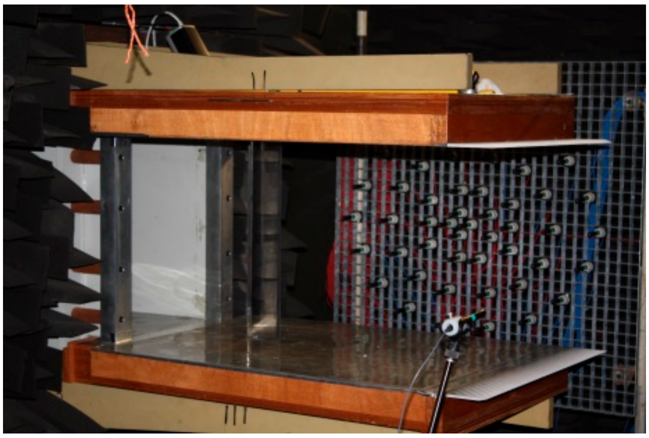

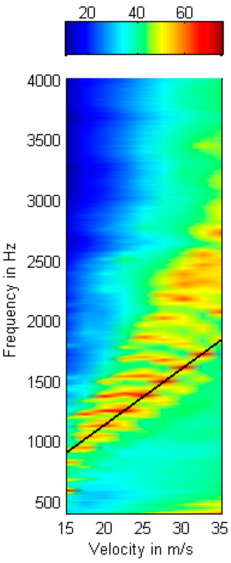

Report no.
NLR-TR-2014-019

Author(s)
F. Gijsman

Report classification
UNCLASSIFIED

Date
February 2014

Knowledge area(s)
Aëro-akoestisch en experimenteel aërodynamisch onderzoek

Descriptor(s)
Noise Propagation
PIV (Particle Image Velocimetry)
Acoustic Measurements
Airfoils

Problem area
Acoustic and PIV measurements were carried out on a NACA0012 profile in NLR's Small Anechoic Wind Tunnel KAT. Airfoil tonal noise is investigated. The main objective was to provide insight into the aeroacoustic source mechanism using PIV measurements.

Description of work
Airfoil tonal noise and flow properties around a NACA0012 profile with a moderately blunt trailing edge for different wind speeds and angles of attack were determined. In order to isolate airfoil tonal noise sources, acoustic measurements were done using a 48-microphone phased array. PIV measurements were performed in a frame of 24 mm by 24 mm around the trailing edge to analyse the source. Laminar boundary layer vortex shedding and trailing edge bluntness vortex shedding were observed and investigated.

Results and conclusions
Intense narrow band tones have been found and both laminar boundary layer- and trailing edge bluntness vortex shedding were observed for velocities of 15 m/s to 35 m/s. From 15 m/s till 27.5 m/s the phenomena worked separately, at higher speeds they start to interact. A linear scaling of the peak frequencies with the velocity is found. All deviations of this pattern can be explained by different flow patterns, shown by the PIV measurements.

Nationaal Lucht- en Ruimtevaartlaboratorium, National Aerospace Laboratory NLR

Anthony Fokkerweg 2, 1059 CM Amsterdam,
P.O. Box 90502, 1006 BM Amsterdam, The Netherlands
Telephone +31 88 511 31 13, Fax +31 88 511 32 10, www.nlr.nl

Nationaal Lucht- en Ruimtevaartlaboratorium

National Aerospace Laboratory NLR

NLR-TR-2014-019

Tonal generation by an airfoil at low to moderate Reynolds numbers

F. Gijsman

Customer	National Aerospace Laboratory NLR
Contract number	-----
Owner	NLR
Division NLR	Aerospace Vehicles
Distribution	Limited
Classification of title	Unclassified
	February 2014

Approved by:

Author	Reviewer	Managing department
F. Gijsman b.a.	M. Tuinstra	J.F. Hakkaart
Date: 12-04-2014	Date: 12-02-2014	Date: 17/2/14

Summary

This test report describes tonal noise generation by an airfoil at low to moderate Reynolds numbers. Acoustic and PIV measurements were carried out on a NACA0012 profile in NLR's Small Anechoic Wind Tunnel KAT. The main objective was to provide insight into the aeroacoustic source mechanism using PIV measurements. Airfoil tonal noise and flow properties around a NACA0012 profile with a moderately blunt trailing edge for different wind speeds and angles of attack were determined. In order to isolate airfoil tonal noise sources, acoustic measurements were done using a 48-microphone phased array. PIV measurements were performed in a frame of 24 mm by 24 mm around the trailing edge to analyse the flow phenomena in the source region. The measurements were carried out for the velocity range of 15 m/s to 35 m/s, representing Reynolds numbers of $1 \cdot 10^5$ to $2.5 \cdot 10^5$. Laminar boundary layer vortex shedding and trailing edge bluntness vortex shedding were observed and investigated. Intense narrow band tones were found that could be related to both laminar boundary layer- and trailing edge bluntness vortex shedding noise. From 15 m/s till 27.5 m/s the phenomena worked separately, at higher speeds they start to interact. A linear scaling of the peak frequencies with the velocity is found. All deviations of this pattern can be explained by different flow patterns, shown by the PIV measurements.

This page is intentionally left blank.

Contents

Abbreviations		**6**
1	**Introduction**	**7**
1.1	Previous research	7
1.2	Theory	8
1.3	Goal	9
2	**Experimental set up**	**10**
2.1	Small Anechoic Wind Tunnel KAT	10
2.2	NACA0012 profile	10
2.3	Acoustic set-up	11
2.4	PIV-measurements	13
3	**Processing**	**14**
3.1	Acoustic data	14
3.1.1	Bandwidth	14
3.1.2	Array processing	14
3.2	PIV data	14
3.2.1	Mean velocity field	14
3.2.2	Power spectrum	15
3.3	Reynolds number	15
4	**Results**	**17**
4.1	Acoustic measurements	17
4.1.1	Tonal peaks	17
4.1.2	Peak amplitudes	21
4.1.3	Trailing edge bluntness vortex shedding	22
4.1.4	Positive versus negative angles of attack	25
4.1.5	Repeatability	26
4.2	PIV measurements	27
4.2.1	Average flow field	27
4.2.2	Power spectral density	32
5	**Conclusions & recommendations**	**36**
6	**References**	**37**

Abbreviations

Latin

c	Chord length [m]
f	Frequency [Hz]
h	Thickness of the blunt part [m]
P	Pressure [N/m^2]
Re	Reynolds number [-]
St	Strouhall number [-]
t	Time [s]
T	Temperature [K]
u, v	Velocity in x- and y-direction [m/s]
$\vec{u}$	Local velocity vector $\begin{Bmatrix} u \\ v \end{Bmatrix}$ [m/s]
U	Free stream velocity [m/s]

Greek

α	Angle of attack [°]
δ	Boundary thickness [m]
δ^*	Displacement thickness [m]
ρ	Density [kg/m^3]
τ	Shear stress [N/m^2]
μ	Viscosity [kg/m/s]

Subscripts

p	Peak
c	Based on chord length
∞	Far field
o	At zero degrees of attack

Abbreviations

KAT	NLR's Small Anechoic Wind Tunnel
PIV	Particle Image Velocimetry
LDA	Laser Doppler Anemometry

1 Introduction

Noise attenuation is an important topic in aviation at the moment. To be able to reduce aeroacoustic noise first an understanding of the aerodynamic phenomena that cause noise needs to be obtained. In this report tonal noise generation by airfoils at low to moderate Reynolds numbers is looked into. A NACA0012 profile with a blunt trailing edge is tested in NLR's Small Anechoic Wind Tunnel (KAT). A combination of laminar boundary layer vortex shedding and trailing edge bluntness vortex shedding noise creates tonal peaks. In paragraph 1.2 a theory behind these mechanisms is explained.

1.1 Previous research

In 1973, Paterson et al.[1] conducted the first research entirely dedicated to tonal noise generation. A remarkable result was a ladder-based structure with an overall trend for the peak frequency of $f_p \sim U^{1.5}$ and a local trend of $f_p \sim U^{0.8}$. Also it was observed that once the flow on the pressure surface of the airfoil transitioned into turbulence, tonal noise could no longer be perceived.

In 1989, Brooks et al.[2] conducted an extensive investigation of airfoil trailing edge noise for the NACA0012. Scaling parameters for boundary thickness, displacement thickness, but also for the effects of laminar boundary layer vortex shedding and trailing edge bluntness vortex shedding are reported.

Lowson et al.[3] made an investigation in 1994 to the latter two phenomena and created a range in which tonal noises appear. An important statement in this paper is that measurements need to be processed with a small bandwidth to investigate laminar boundary layer vortex shedding; since otherwise some tonal noises will not be observed. Also was expected that the two phenomena would work together at the moment described in (Eq.1).

$$\frac{h}{c} = \frac{12.5}{Re^{0.5}} - 0.015Re^{-0.2} \qquad \text{(Eq.1)}$$

In this equation h is the thickness of the blunt trailing edge, c is the chord length and Re is the Reynolds number based on the chord length. This formula is found by combining relations found for laminar boundary layer vortex shedding and trailing edge bluntness vortex shedding. Nash et al.[4] visualized the flow by Laser Doppler Anemometry (LDA), and showed that the flow was highly influenced by mean velocity and r.m.s. fluctuation profiles on the pressure surface of the airfoil.

1.2 Theory

In this paragraph a theory behind the origin of the vortex shedding is explained for laminar boundary layer vortex shedding and trailing edge bluntness vortex shedding. It has to be stated that this theory is not proven.

1.2.1 Origin of laminar boundary layer vortex shedding

To explain laminar boundary layer vortex shedding, there is started with the momentum equation of the Navier-Stokes equations stated in (Eq.2)

$$\frac{\partial(\rho\vec{u})}{\partial t} = -\nabla P - \nabla(\rho\vec{u})\vec{u} - \nabla\tau + \rho f \qquad \textit{(Eq.2)}$$

A 2D, incompressible Newtonian flow with no external forces is assumed for the flow in a boundary layer, this results in (Eq.3)

$$\rho\frac{\partial(\rho\vec{u})}{\partial t} + \rho u\frac{\partial\vec{u}}{\partial x} + \rho v\frac{\partial\vec{u}}{\partial y} = -\nabla P + \mu\nabla^2\vec{u} \qquad \textit{(Eq.3)}$$

Looking for the momentum equation in x-direction leaves (Eq.4)

$$\rho\frac{\partial(\rho u)}{\partial t} + \rho u\frac{\partial u}{\partial x} + \rho v\frac{\partial u}{\partial y} = -\frac{\partial p}{\partial x} + \mu\left(\frac{\partial^2 u}{\partial y^2} + \frac{\partial^2 u}{\partial x^2}\right) \qquad \textit{(Eq.4)}$$

Making use of the boundary layer approximation stated in equation (Eq.5) and looking at the boundary condition at the wall, where $\vec{u}$ equals zero, remains (Eq.6).

$$\frac{\partial^2 u}{\partial x^2} \ll \frac{\partial^2 u}{\partial y^2} \qquad \textit{(Eq. 5)}$$

$$\left.\frac{\partial^2 u}{dy^2}\right|_{y=0} = \frac{1}{\mu}\frac{dp}{dx} \qquad \textit{(Eq. 6)}$$

This means that if the curvature of the profile is positive, the pressure increases in x-direction. The velocity profile will transpose from the normal velocity profile as shape A in Figure 1 to shape C in Figure 1. When the profile gets this shape the inviscid-stability theory says that the boundary layer becomes possibly unstable. In the case of a NACA0012 profile the curvature is approximately zero, at some places it becomes slightly positive. This causes instability.

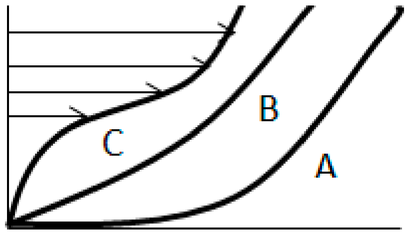

Figure 1 Velocity profiles

At slight disturbances the instable flow profile starts to separate Tollmien-Schlichting vortices. These two dimensional Tollmien-Schlichting instability waves generate tonal noise.

1.2.2 Origin of trailing edge bluntness vortex shedding

Trailing edge bluntness vortex shedding is established to be an important air foil self-noise source. Because of the wake behind the trailing edge a Karman Vortex Street is created.

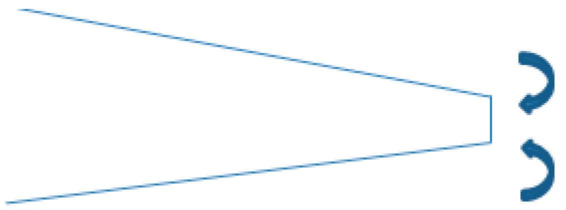

Figure 2 Trailing edge bluntness vortex shedding

1.3 Goal

In this research PIV-measurements are used to study the flow in the trailing edge region. These results are compared with the acoustics. The goal is to provide insight into the aeroacoustic source mechanism using PIV measurements.

This report is outlined as follows: in chapter 2 the experimental set up is treated. This is followed by chapter 3 in which the processing of the data is explained. In chapter 4 the acoustic and PIV results are presented. The conclusions are provided in chapter 5.

2 Experimental set up

In this chapter the experimental set up will be described. The conditions of the wind tunnel, NACA0012 profile, acoustic equipment and PIV-measurements will be discussed.

2.1 Small Anechoic Wind Tunnel KAT

The tests were performed in NLR's Small Anechoic Wind Tunnel KAT. The KAT is an open circuit, open jet wind tunnel. The nozzle has a cross section of 0.51 m by 0.38 m and is placed in a 5.5 m by 5.5 m by 2.5 m room completely covered with 0.5 m foam wedges, yielding 99 % acoustic wave absorption above 500 Hz. Two horizontal endplates are mounted to the upper and lower sides of the nozzle, which provides a semi-open test section. To suppress reflections a 55 mm layer of sound absorbing foam covered by a 5 % open perforated plate is acoustically lined with the endplates. In Figure 3 a picture of the facility is shown.

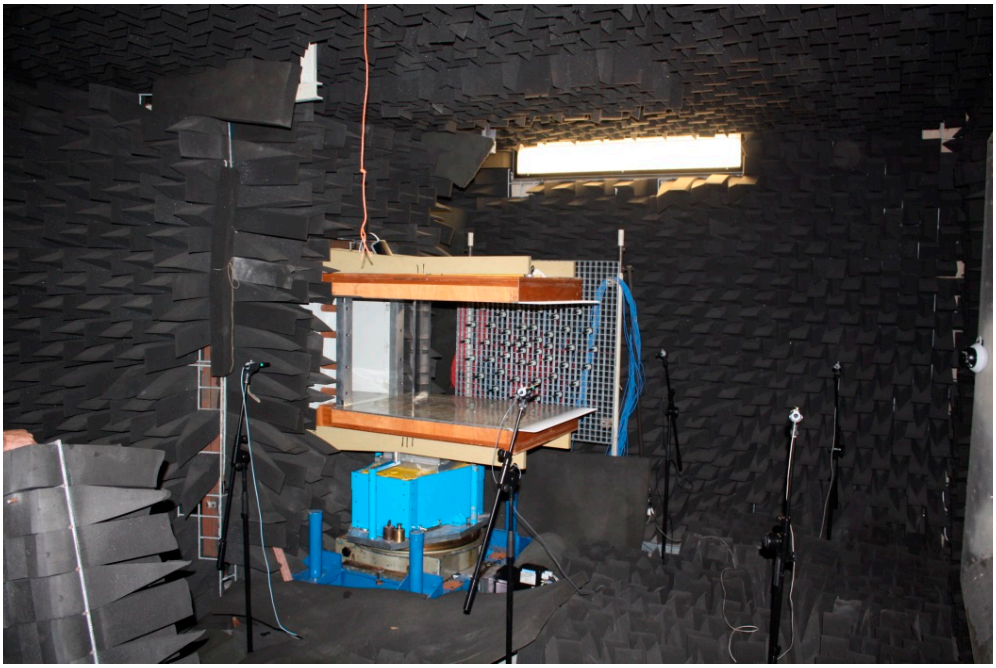

Figure 3 Set up in the KAT for the acoustic tests

2.2 NACA0012 profile

A NACA0012 aerofoil with a chord length of 0.10 m is used. A transparent profile made of plexiglass is chosen since this material allows illumination of particles on both sides of the airfoil during PIV-measurements. To be sure the material would not break during the milling process a trailing edge thickness of 0.8 mm is produced. A steel mounting interface is placed at the bottom of the profile. This can be seen in Figure 4. The interface was placed on a turntable to be able to measure under positive and negative angles of attack as shown in Figure 5.

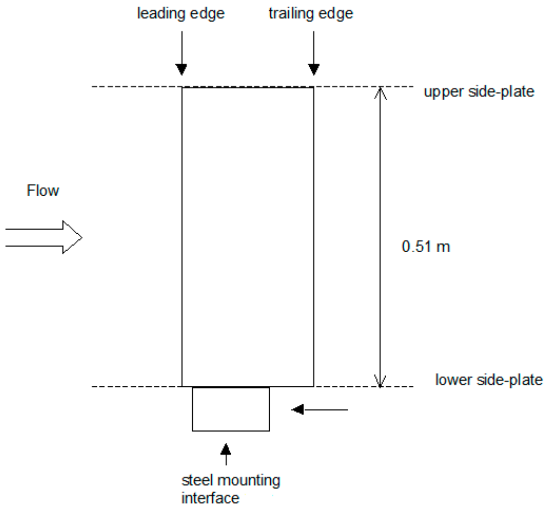

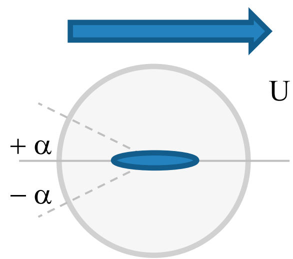

Figure 4 Sketch of the NACA0012 profile

Figure 5 Position of the airfoil on the turntable

2.3 Acoustic set-up

The acoustic setup in the tunnel was shown in Figure 3. For the measurements six far field microphones and an array of 48 ½-inch microphones (type LinearX M51) are used. The array was place outside the tunnel flow at a distance of 0.8 meter from the tunnel axis, as shown in Figure 6. In Figure 7 the position of the microphones in the array is shown.

During the acoustic measurements angles of attack from minus eight to eight degrees are investigated with increments of two degrees. Velocities from 15 m/s to 35 m/s are used in the acoustic measurements. For all positive angles of attack the velocity was increased in increments of 2.5 m/s, for the negative angles of attack the increments were 5 m/s.

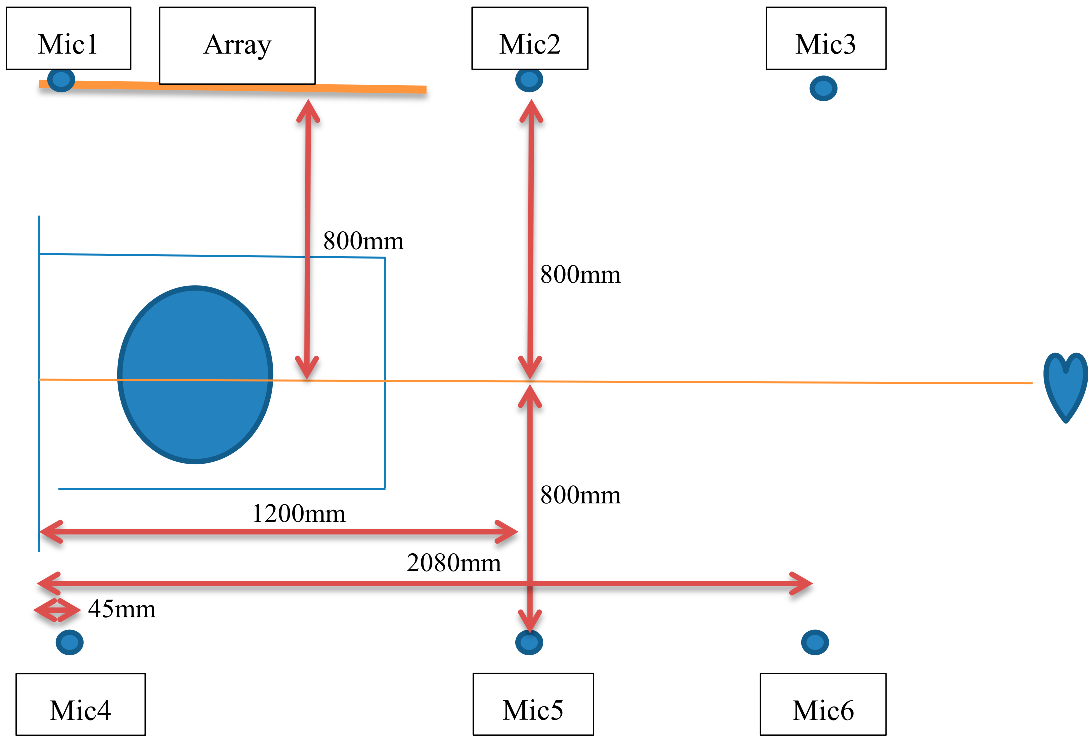

Figure 6 Position of the microphones in the wind tunnel

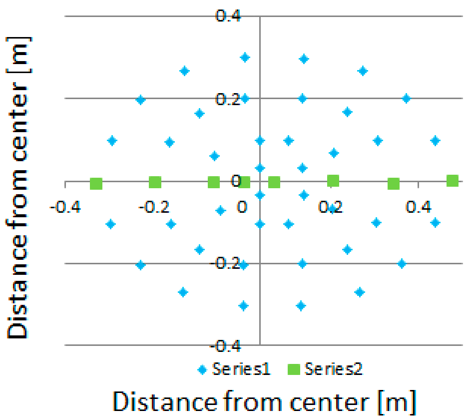

Figure 7 Microphone positions in the array

2.4 PIV-measurements

In order to investigate the flow around the trailing edge, Particle Image Velocimetry was used. The flow was seeded using a HAAGEN Etna Smoke Generator, using HAAGEN smoke fluid. These particles are illuminated by a laser; in this case a Litron LDY300 high speed Laser, which yields 30 mJ/pulse at 1 kHz output. The LaVision HighSpeedStar 8 high sensitivity, megapixel resolution digital camera, is used to obtain the flow in the different time steps. This camera has a resolution of 1024 px by 1024 px. During the tests a frame rate of 2 kHz was used. For each measurement half a second of data was obtained, resulting in 1000 observations per measurement.

The tests were performed for angles of attack of two, four and six degrees. Velocities from 15 m/s till 35 m/s with increments of 5 m/s were used. The software used to process PIV data was DaVis 8.

3 Processing

3.1 Acoustic data

3.1.1 Bandwidth

The acoustic data are processed with two different frequency steps; a small bandwidth set with a frequency step of 5 Hz and a 1/3 octave band in which the broad bandwidth is looked into. In this report the results of the small band frequencies are mostly used.

3.1.2 Array processing

The acoustic data from the array microphones were measured using the VIPER data-acquisition system. The data were acquired with a sample frequency of 81.92 kHz for a measurement time of 30 seconds. The array data were processed using the SOLACAN software, which produces acoustic source maps in 1/3-octave bands using conventional beam forming. In this way, noise originating from the model is separated from background noise. Furthermore the acoustic data are imported and processed in MatLab.

3.2 PIV data

The PIV data were processed by LaVions DaVis 8. From the measurements, the 1000 observations were correlated using interrogation windows of 24 px by 24 px with 50% overlap. This results in a vector field of 86 by 86 vectors. The field of view is centered around the trailing edge in a 24 mm by 24 mm frame.

3.2.1 Mean velocity field

From the vector data a mean velocity field is calculated by DaVis 8, these results are imported in MatLab. As output DaVis gives four 86 by 86 matrices, consisting of two position and two velocity component matrices.

In MatLab these results were analysed to find the boundary thickness and displacement thickness. To be able to measure these parameters the position of the boundary layer needs to be stated. The boundary layer is assumed to be present when the velocity is at 99% of the far field velocity. Problem is that the flow is decelerating in the captured domain. To deal with this a local edge velocity far enough from the airfoil to be outside the boundary layer is taken as reference. The boundary layer is assumed to be at the position where the velocity equals 99% of the edge velocity. An example of the processed data is shown in Figure 8.

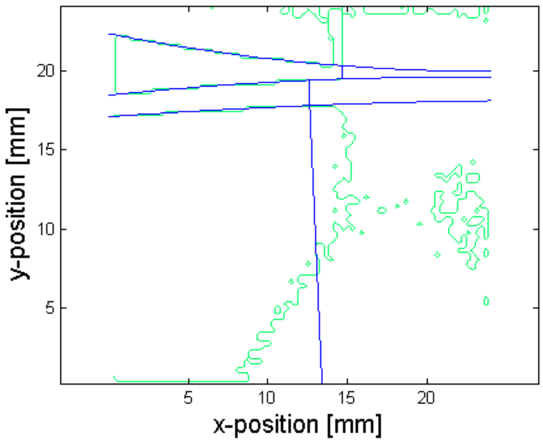

Figure 8 Sketch of the profile and boundary layer processed in MatLab

3.2.2 Power spectrum

Also the power spectral density of the velocity is obtained by DaVis 8. Because of a frame rate of 2 kHz a Nyquist frequency of 1000 Hz is obtained. A plot over whole the domain is made to obtain information of the origin of the airfoil tonal noise. Also some positions around the trailing edge are investigated in MatLab, using the function pwelch() and inserting a hanning window.

3.3 Reynolds number

To be able to compare the results with other research the Reynolds number is obtained. As length size usually is taken the chord length.

$$Re_c = \frac{\rho U c}{\mu} \; (Eq.7)$$

First the density and viscosity are looked into. The viscosity is determined by Sutherland's law, with as reference conditions $\mu_0 = 1.7894 \cdot 10^{-5} \frac{kg}{ms}$ and $T_0 = 288.16K$ at atmospheric pressure. These conditions are found in reference [5].
Sutherland's law sounds is stated in (Eq.8).

$$\frac{\mu}{\mu_0} = \left(\frac{T}{T_0}\right)^{\frac{3}{2}} \frac{T_0 + 110}{T + 110} \; (Eq.8)$$

The density can be obtained by the ideal gas law. The average temperature of $T = 20°C$ during the measurements leads to the values $\mu = 1.8134 \cdot 10^{-5} \frac{kg}{ms}$ and $\rho = 1.204 \frac{kg}{m^3}$ during the measurements. The Reynolds numbers are stated in Table 1.

Table 1 Reynolds number based on chord length at the different velocities

Velocity (m/s)	Re_c(-)
15	$0.96 \cdot 10^5$
20	$1.32 \cdot 10^5$
25	$1.66 \cdot 10^5$
30	$1.99 \cdot 10^5$
35	$2.32 \cdot 10^5$

4 Results

This section discusses the results of the measurements. First the acoustics will be discussed and then the PIV results are provided.

4.1 Acoustic measurements

Out of the acoustic measurements the sound spectra are obtained, these results are shown in Figure 9, where the spectra are given as a function of velocity.

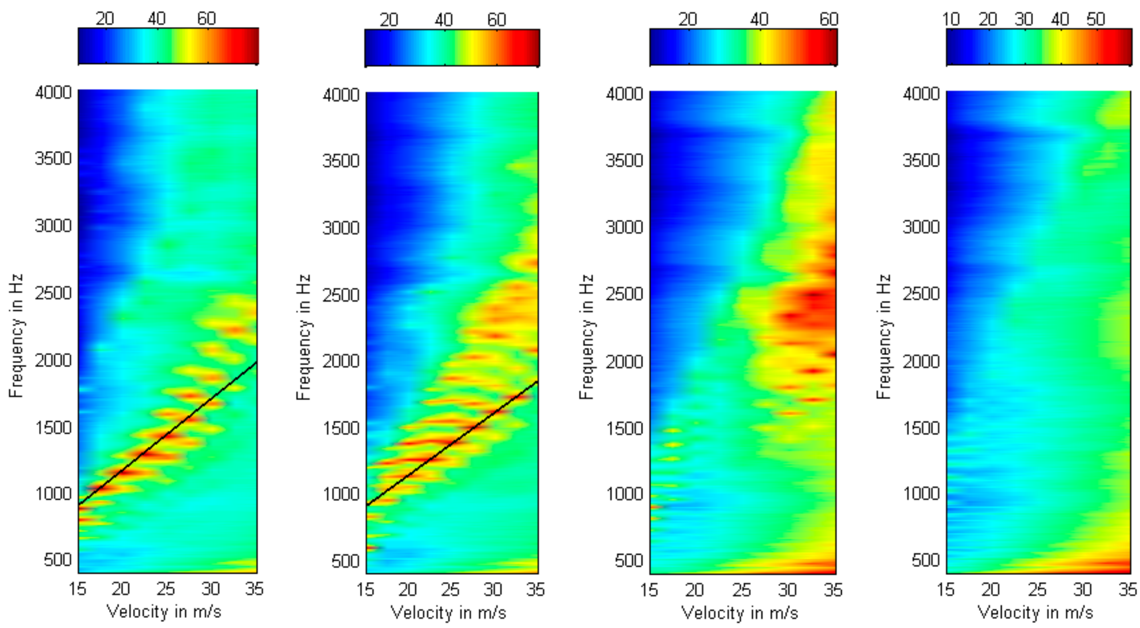

Figure 9 Frequency versus velocity plots with $\alpha = 0, 2, 4, 6$ degrees. The colors represent the noise level produced at that point in dB. A Δf of 5 Hz and a ΔU of 2.5 m/s is used

4.1.1 Tonal peaks

The red peaks in Figure 9 represent the tonal components. At angles of attack of zero and two degrees multiple peaks appear at a single velocity. Those peaks are found in a narrow frequency range and the frequency of the peak increases with velocity. At two degrees the range gets broader at higher velocities. A ladder based structure can be obtained in peak frequencies in both domains.

At an angle of attack of four degrees no tonal components appear for velocities lower than 30 m/s. For higher velocities multiple tonal peaks appear. At these conditions also a raise of the noise intensity over the narrow range in which tonal components appear is shown. At an angle of attack of six degrees no tonal noise can be seen.

4.1.1.1 Ladder structure

A ladder based structure is observed in Figure 9. The steps do not compare with the ladder-based structure described by Patterson et al.[1] which describes a relation between the maximum peak frequencies. This is because of the course resolution of measurements in velocity direction. In Figure 10 the sound spectra with velocities of 20, 22.5 and 25 m/s are plotted. At the following step in velocity the frequency of other tonal peaks ends up at the same frequency, causing the graph to interpolate with different values. To be able to find the right relation for peak frequencies the same peaks are interpolated in MatLab as described in chapter 4.1.1.2, from these interpolations (Eq.3) and (Eq.4) are plotted in Figure 9.

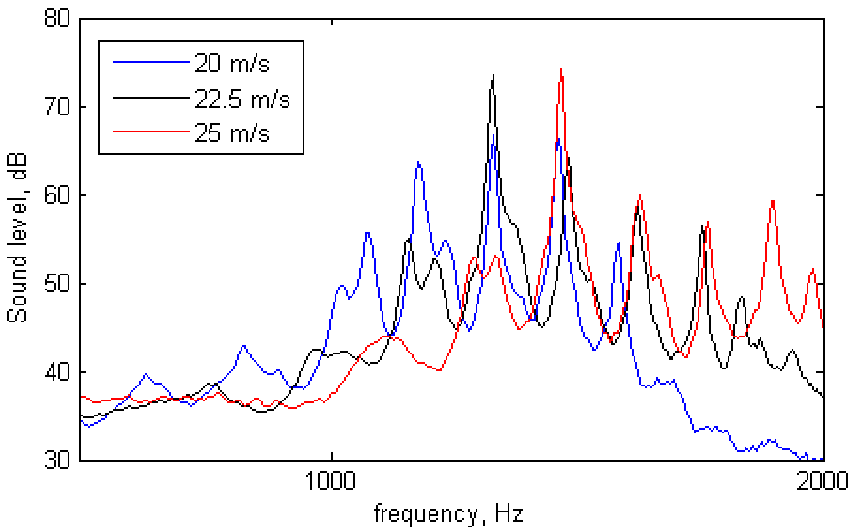

Figure 10   Sound spectra with velocities 20, 22.5 and 25 m/s and an angle of attack of 2 degrees. The frequency axis is logarithmic

4.1.1.2 Peak frequency trends

To spot a relation in the measurements, the maximum tonal peaks are looked into. In Figure 11 the peak frequencies are plotted versus the velocity in a logarithmic scale.
In Patterson et al.[1] a ladder-based structure is found with the overall trend of $f_p \sim U^{1.5}$. A local dependence of the peak frequency with $U^{0.8}$ is obtained. To compare this with the measurements in this report the two dependencies are plotted through the peak frequencies. The best fit for a power function is $f \sim U^{0.915}$ at zero angle of attack. Since the results look linear, a linear fit is tried and appeared to have the same accuracy with a frequency described in (Eq.9)

$$f = 53.64 \cdot U + 100.8 \text{ (Eq. 9)}$$

At an angle of attack of two degrees a fit corresponding to the power function results in $f \sim U^{0.862}$, but a linear relation fits almost as good. This relation is shown in (Eq.10).

$$f = 47U + 202.5 \ (Eq.10)$$

Looking at an angle of attack of four degree the peak frequencies appear at higher frequencies than the peaks at lower angles of attack. It looks like these results belong to the next rung in the ladder-like structure described by Patterson et al.[1]

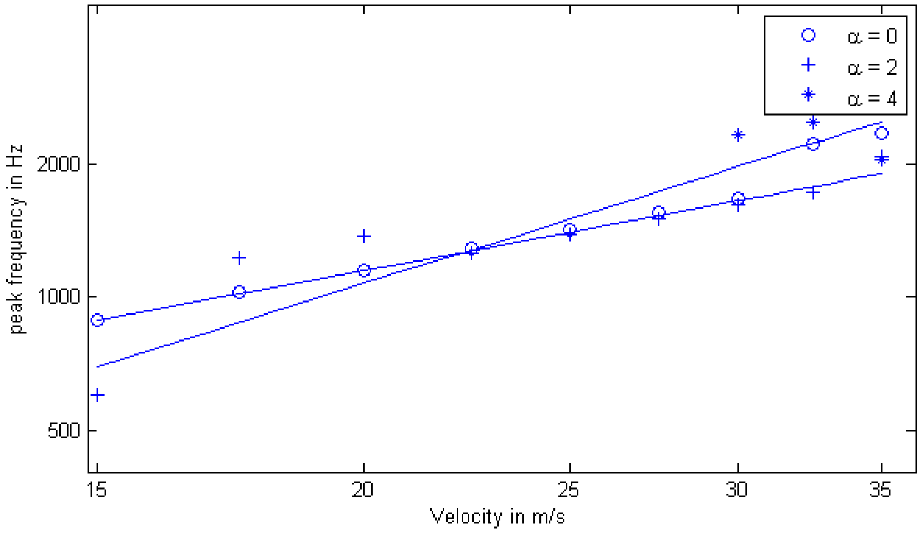

Figure 11 Representation of the positions with maximum tonal noise. A interpolation with the dependencies $f_p \sim U^{1.5}$ and $f_p \sim U^{0.8}$ is added

To obtain the relation in (Eq.10) the measurements at 15, 17.5 and 20 m/s were be neglected. To find out why these peak frequencies are not in line with the others the sound spectra are further investigated.

The frequency of the peak with $\alpha = 2°$ at 15 m/s is lower than expected, while the frequencies of the peaks at 17.5 m/s and 20 m/s are higher than expected. In Figure 9 it was already shown that more peaks were present in a narrow region, to get a better insight in the phenomena the spectra are pointed out in Figure 12. These spectra are scaled with the linear relation found in (Eq.10). At the sound spectra of 17.5 and 20 m/s similar peak frequencies are found, only another peak becomes dominant. This causes a deviation of the linear fit.
The domain in which the peaks at 15 m/s appear is broader that the domain at higher velocities. Apparently a different source mechanism is at work.

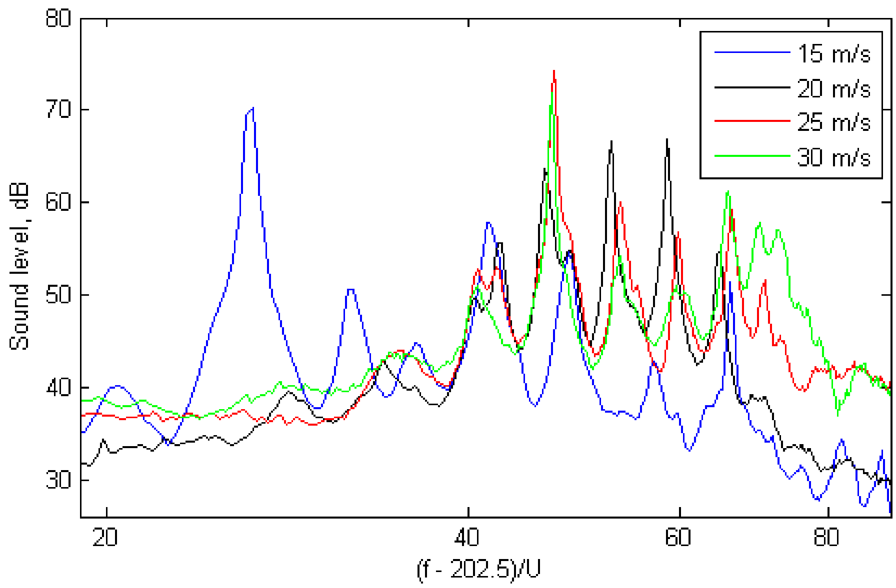

Figure 12 Scaled sound spectra for the velocity of 15, 20, 25 and 30 m/s at $\alpha = 2°$, with f as frequency and U as far field velocity

4.1.1.3 Tonal noise range

Lowson et al. [3] showed the region in which the tonal noise was found based on the Reynolds number and the angle of attack. This graph is shown in Figure 13. In this graph the limit between the tone and no tone conditions is shown. Also a line with maximum noise level is presented.

To implement the results into Figure 13 a wind tunnel correction is made. The angle of attack α_* represents the angle in free air required to give the same lift as α_t would give in a tunnel. Out of measurements of Brooks [2] the relation of $\alpha_*/\alpha_t = 0.62$ is found for a chord length of 0.10 m, which was used in our results to correct. Our results were compared with that of Lowson, as shown in Figure 13.

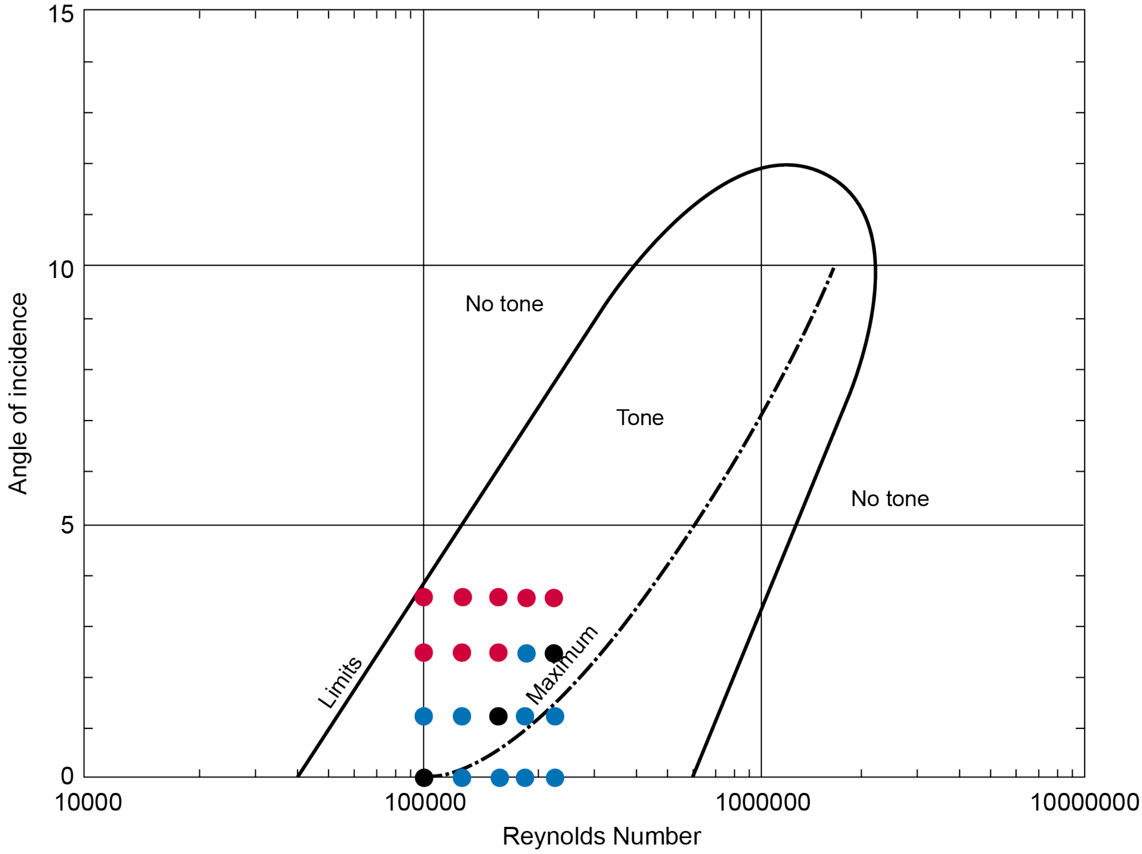

Figure 13 Range where tonal noise can be obtained, shown by Lowson et al.[3]. The results of this investigation are added. The red dots in the profile represent no tones. At the position of the blue points tonal noise exists and at the black points a maximum tone is obtained for that angle of attack

From the implemented measurements can be concluded that the measured range of tonal noises is smaller. This could be due to other turbulent conditions in the wind tunnel, a wrong wind tunnel correction for this tunnel or this might suggests that the profile was not smooth enough to obtain all tones. Most importantly it shows the sensitivity of this configuration to wind tunnel environment.

4.1.2 Peak amplitudes

Also there is looked at the amplitudes of the peaks. Because of the many different flow parameters it is hard to find a correlation. Correlations found by Brooks at al.[2] do not compare to the results. In Figure 13 a line of maximum tonal noise is shown. This can be compared with the maximum peaks in our measurements per angle of attack. A similar trend is observed, only the maximum tones appear at a lower Reynolds number.

4.1.3 Trailing edge bluntness vortex shedding

In Brooks et al. [2] is described that blunt trailing edge noise scales with

$$St_p = \frac{f_p h}{U} \approx 0.11$$

The frequency in this survey is collected in a 1/3 octave bandwidth and gave peaks that could be scaled as shown in Figure 14. A hump in the pattern appears in which a peak frequency is shown. The place of the peak in the hump changes per velocity; this makes it hard to scale with the Strouhall number. If there is looked at the average Strouhall number in these results, it is 0.075 which is smaller than in the results of Brooks[2].

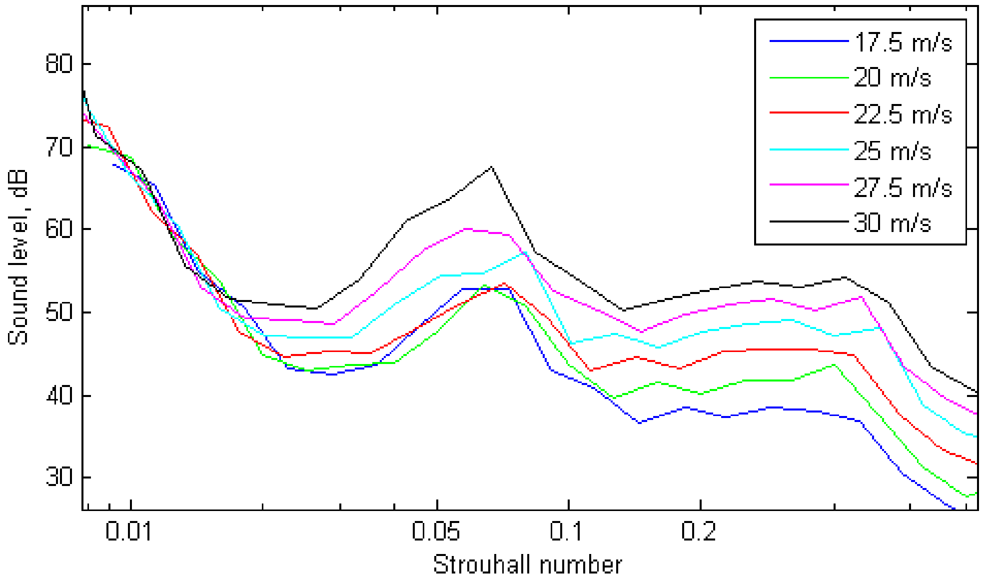

Figure 14 Sound level versus Strouhall number for an angle of attack of 4 degrees

To get a better insight in the phenomena measurements are also made in a small bandwidth, a sound spectrum in this case is shown in Figure 15. No clear tonal noise is visible, but it looks more like a hump in the area in which vortex shedding appears. This means that not one value of the Strouhall number can be obtained, but a region in which trailing edge bluntness vortex shedding appears.

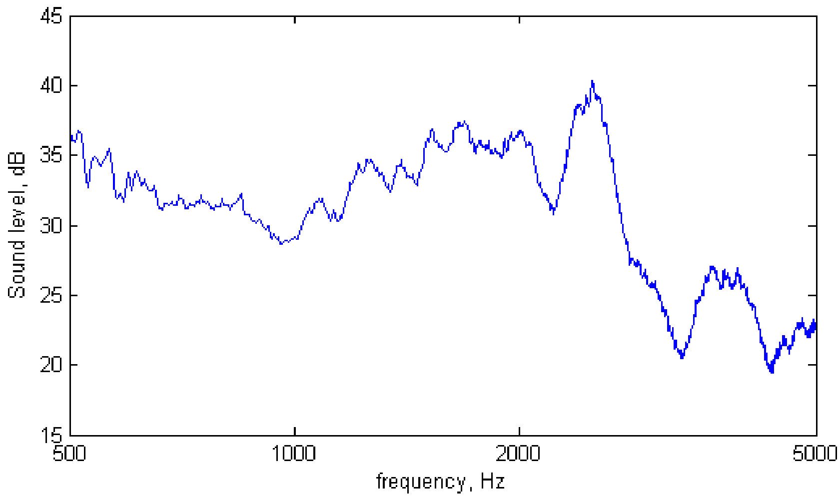

Figure 15 Sound spectrum at an angle of attack of four degrees and a velocity of 25 m/s

Lowson et al.[3] stated that the trailing edge bluntness vortex shedding would combine with laminar boundary layer vortex shedding at

$$\frac{h}{c} = \frac{12.5}{Re^{0.5}} - 0.015Re^{-0.2} \qquad \text{(Eq.1)}$$

This formula is made by combining relations found for laminar boundary layer vortex shedding and trailing edge bluntness vortex shedding.

Looking at the Reynolds numbers in our experiments, this would give a needed trailing edge thickness h of at least 2.5 mm. Remarkably, despite of the trailing edge thickness of just 0.8 mm, at higher velocities the trailing edge bluntness vortex shedding noise does work together with the laminar boundary vortex shedding noise. A sound spectrum is shown in Figure 16. Three peaks appear in this situation. The peaks that could be seen at laminar boundary shedding are pushed up by the bluntness effect, which causes that secondary, and even tertiary peaks become larger than the originally dominant peak. This could be a reason for the higher level in the ladder-based structure described by Patterson et al.[1]

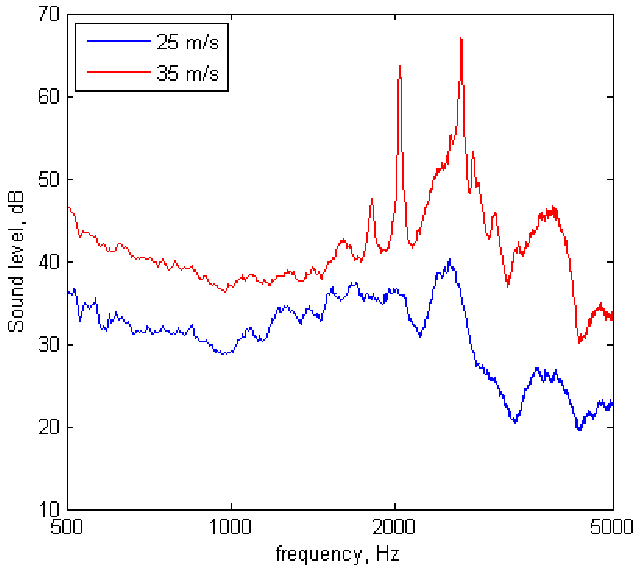

Figure 16 Sound spectrum at $\alpha = 4°$ and velocities of 25 m/s and 35 m/s

Another transition where trailing edge bluntness vortex shedding seems to take part into the process is at an angle of attack of two degrees between 30 m/s and 35 m/s. In Figure 17 the two spectra are shown. What can be observed is that the peaks at the velocity of 30 m/s all start at approximately the same level, while at 35 m/s the spectrum has a bump and peaks at higher frequencies start at a higher sound level. It can also be obtained the tonal peak at 30 m/s is louder.

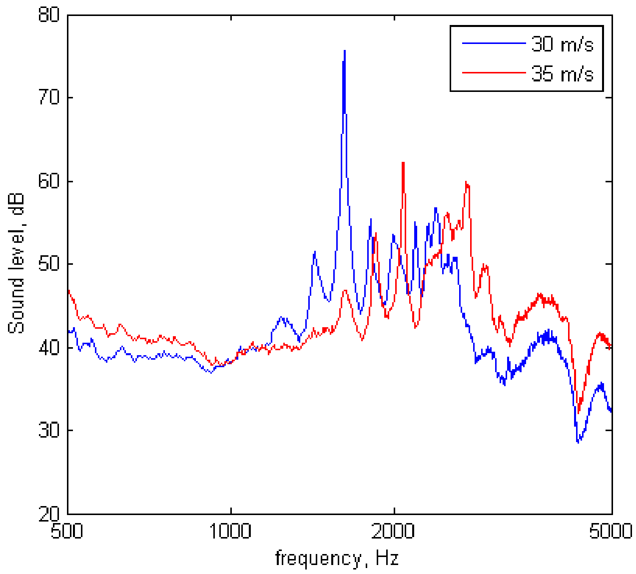

Figure 17 Sound spectrum at $\alpha = 2°$ and velocities of 30 m/s and 35 m/s

In trailing edge bluntness vortex shedding directivity is a factor. To give a view in which direction trailing edge bluntness sends off the most noise in Figure 18 the sum of the noise levels in the hump is compared with the angle between the chord line and the position of the microphone. Results observed by the microphones of series 2 in Figure 7 are investigated. A correction for the distance to the trailing edge is made, where the distance perpendicular from the profile to the microphones is taken as a reference distance. In the plot can be seen that most of the trailing edge bluntness noise is transmitted upstream in the flow.

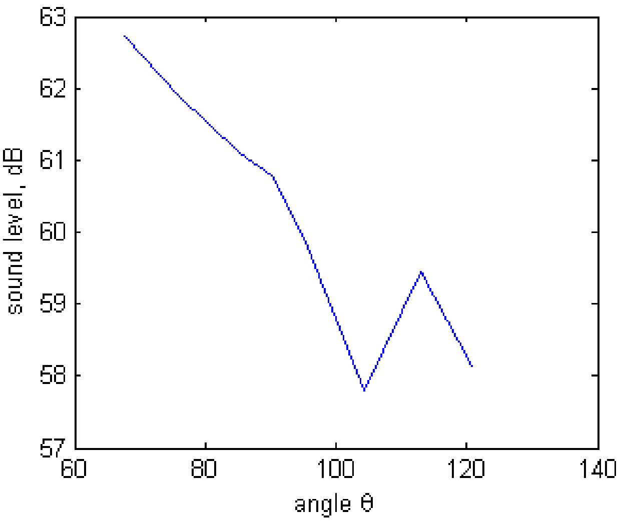

Figure 18 Sound level in the hump set out versus the angle θ

4.1.4 Positive versus negative angles of attack

The profile is symmetric, there is looked if the results are symmetric too. The profile is looked into in a negative and positive angle of attack. In Figure 19 the results are shown. In the case with $\alpha = -2° \; or \; 2°$ the pattern is similar, but peak levels vary strongly. It looks like two different phenomena take place. We are not sure what causes these differences.

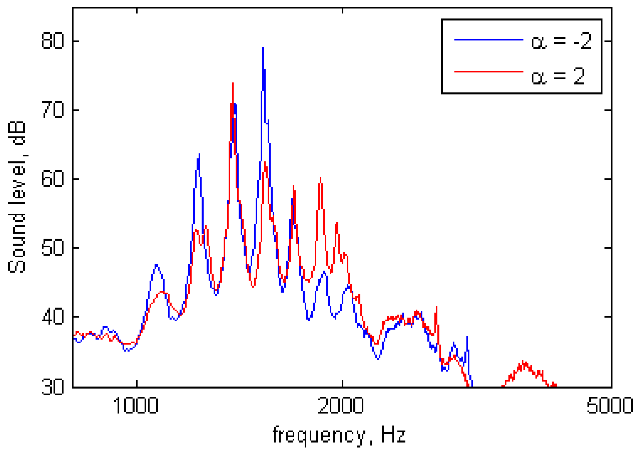

Figure 19 Sound spectra for 30 m/s and $\alpha = -2°$ and $\alpha = 2°$

4.1.5 Repeatability

To check if the results are repeatable the measements were done again at a velocity of 30 m/s. Using angles of attack from minus eight to plus eight degrees, and back the other way around. At the places where the both phenomena work seperately the phenomena are highly repeatable, but when they do work together different peaksizes are obtained. The differences are not in the peak frequencies, but in the sound level. These differences can make another peak dominant, which is shown in Figure 20.

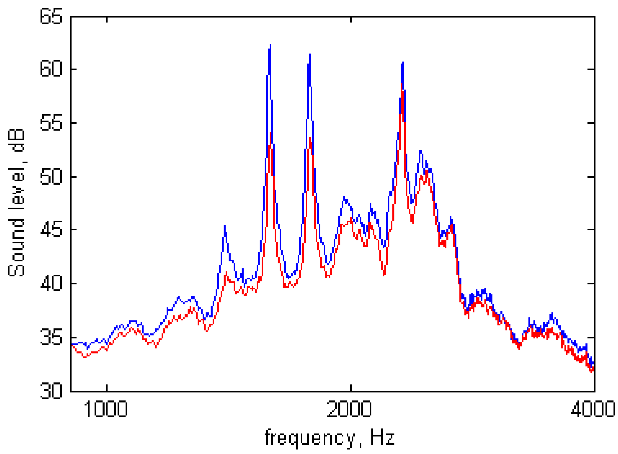

Figure 20 Sound spectra at two different measurements for 30 m/s and α=4°

4.2 PIV measurements

To find an explanation for the acoustic behaviour PIV measurements are performed. First there will be looked into the average flow field, where after several power spectral density and proper orthogonal decomposition plots are shown.

4.2.1 Average flow field

In chapter 3 the processing of the data for an average field is explained. Now the results will be discussed. In Figure 21 an example of a flow pattern found in Davis 8 is shown. It the background of this plot the velocity in x-direction is shown. The build-up of velocity in the boundary layer can clearly be seen.

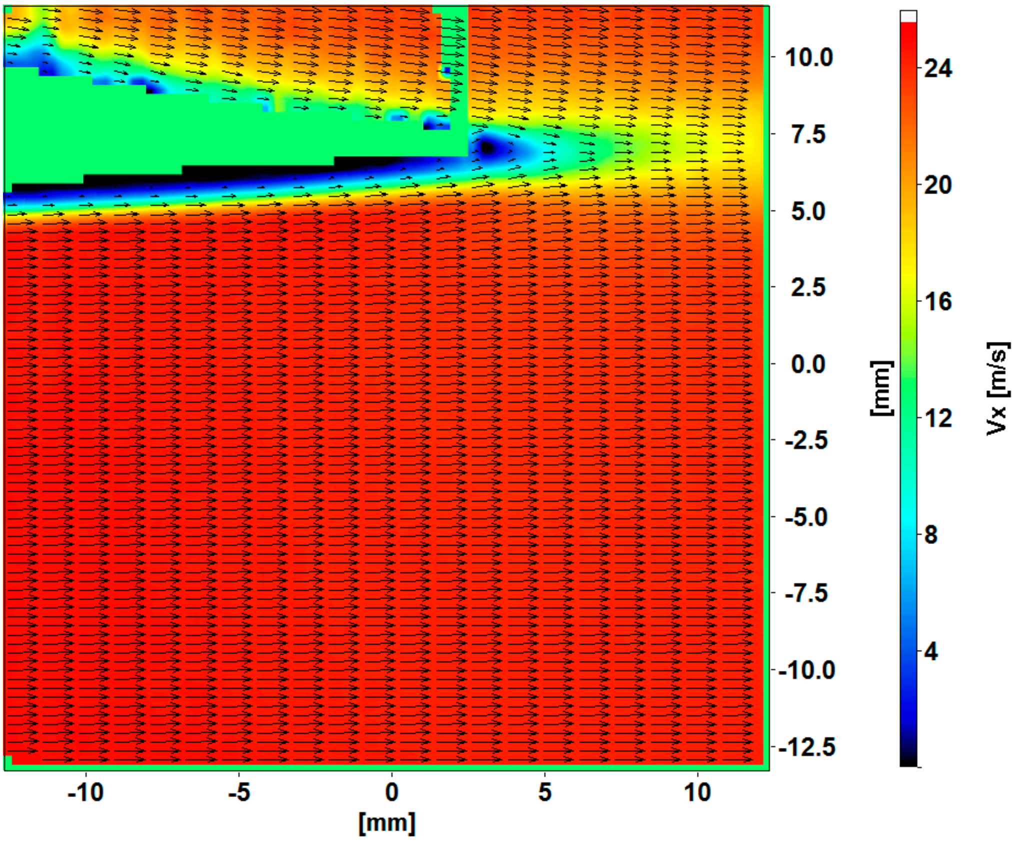

Figure 21 Vector field around the airfoil for a velocity of 25 m/s and angle of attack of 2°

4.2.1.1 Velocity boundary layer profiles

First the velocity profiles in the boundary layer and the way they evolve over the profile is discussed. The instable flow pattern discussed in chapter 1.2.1 is clearly visible at all measurements. In Figure 22 the velocity profiles at an angle of attack of two degrees are shown for velocities of 15 m/s, 25 m/s and 35 m/s. It is remarkable that the velocity profile reattaches before the trailing edge at the velocity of 35 m/s. Comparing with the acoustic data; this is the domain where the sound spectrum in Figure 16 stated that the laminar boundary layer vortex shedding and trailing edge bluntness vortex shedding seem to work together. To confirm that this velocity profile can be obtained in all situations where these phenomena work together, the velocity fields at an angle of attack of four degrees are obtained. These are shown in Figure 23, the same pattern appears.

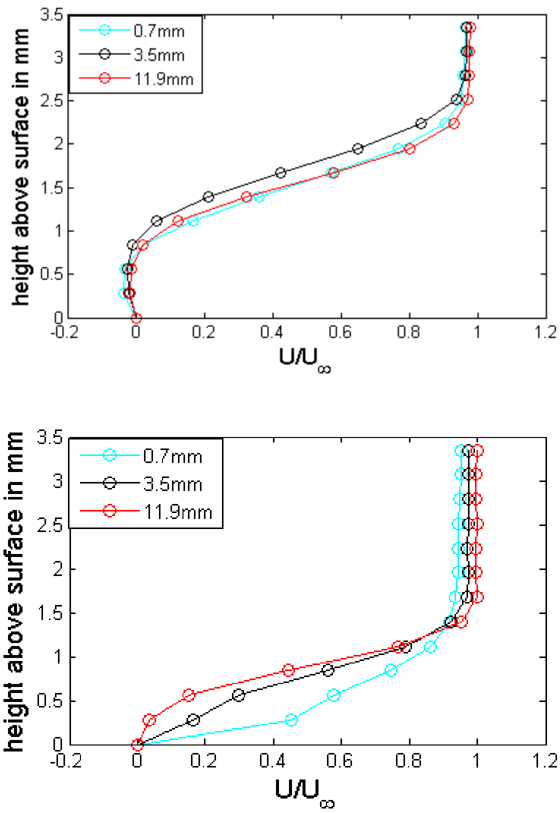

Figure 22 Velocity profiles at an angle of attack of two degrees at velocities of 15 (upper left), 25(upper right) and 35 m/s. In the legend the distance upstream from the trailing edge is stated

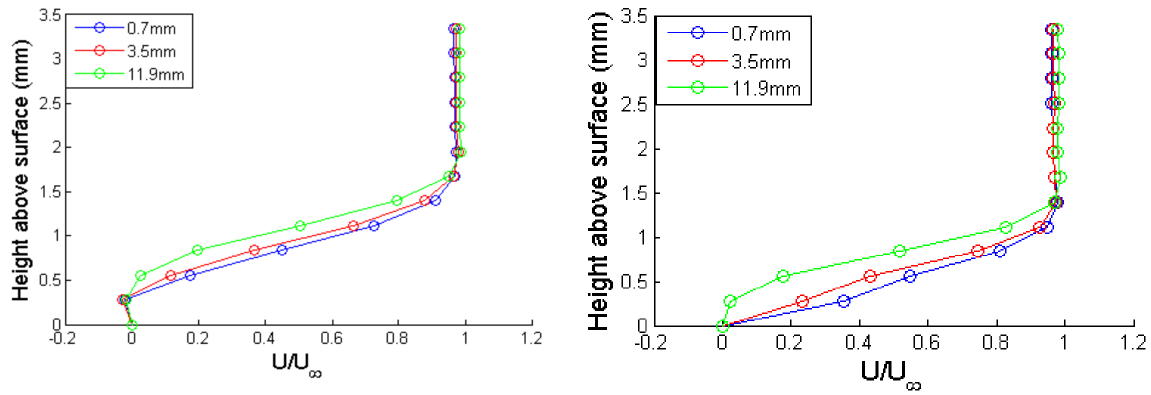

Figure 23 Velocity profiles at an angle of attack of four degrees at velocities of 25 m/s and 35 m/s. In the legend the distance upstream from the trailing edge is stated

4.2.1.2 Boundary thickness

In chapter 3.2.1 is explained how the place of the boundary layer is obtained. With a perpendicular line from the surface to the boundary layer the boundary layer thickness can be obtained. These results are shown in Table 2. In earlier research of Brooks et al.[2] a scaling rule for boundary thickness is obtained. The scaling is shown in (Eq.11)

$$\frac{\delta_0}{c} = 10^{\left[1.6569 - 0.9045 \log(R_c) + 0.0596 (\log(R_c))^2\right]} (Eq. 11)$$

In this equation, δ_0 equals the boundary thickness at zero degree angle of attack, c is the chord length and R_c is the Reynolds number based on chord length.

As a correction for the angle of attack the approximation stated in (Eq.12) is made, with α_* representing the angle in free air required to give the same lift as α_t would give in the tunnel. δ_p states the boundary thickness on the pressure surface of the airfoil.

$$\frac{\delta_p}{\delta_0} = 10^{\left[-0.04175\alpha_* + 0.00106\alpha_*^{\,2}\right]} \ (Eq. 12)$$

Table 2 Flow parameters for $\alpha = 2°, c = 0.10\ m$

Velocity (m/s)	Re_c $(-)$	δ_0/c $(-)$	$\delta_{p,exp}$ (mm)	$\delta_{p,found}$ (mm)	$\delta^*_{p,exp}$ (mm)	$\delta^*_{p,found}$ (mm)
15	$0.96 \cdot 10^5$	0.0417	3.8	2.4	0.83	1.6
20	$1.32 \cdot 10^5$	0.0383	3.4	1.9	0.72	1.1
25	$1.66 \cdot 10^5$	0.0360	3.2	1.6	0.65	0.8
30	$1.99 \cdot 10^5$	0.0342	3.1	1.3	0.60	0.6
35	$2.32 \cdot 10^5$	0.0327	2.9	1.2	0.57	0.4

The results are stated in Table 2. The found thickness is less than found in the relations of Brooks et al.[2]; also the trend of decreasing boundary thickness is faster than expected.

4.2.1.3 Displacement thickness

Brooks et al.[2] also found a scaling rule for displacement thickness is obtained. The scaling is shown in (Eq.13)

$$\frac{\delta_0^*}{c} = 10^{\left[3.0187 - 1.5397 \log(R_c) + 0.1059 (\log(R_c))^2\right]} (Eq. 13)$$

In this equation, δ_0^* equals the displacement thickness at zero degree angle of attack.

As a correction for the angle of attack the approximation stated in (Eq.14) is made, δ_p^* states the displacement thickness on the pressure surface.

$$\frac{\delta_p^*}{\delta_0^*} = 10^{[-0.0432\alpha_* + 0.00113\alpha_*^2]} \; (Eq. 14)$$

Results are adjusted in Table 2.

To obtain the displacement thickness is our results; first a curve fit is performed with the measured data in the boundary layer as can be seen in Figure 24.

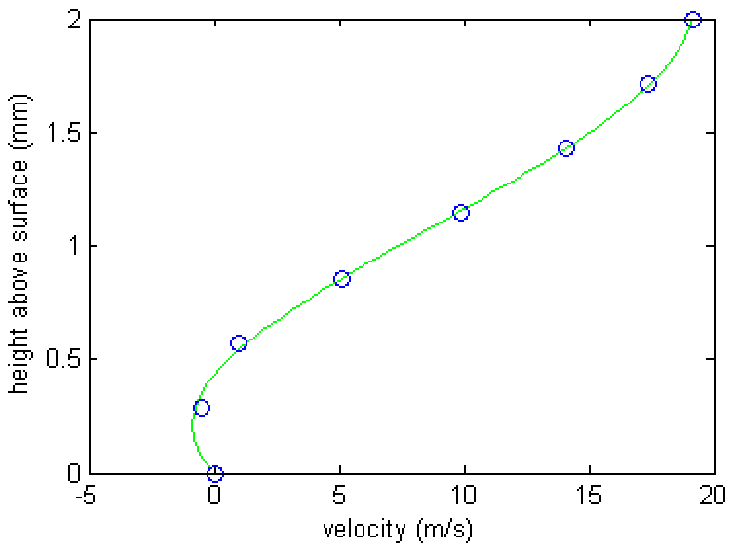

Figure 24 Velocity profile on the pressure side at 20 m/s, 1.3 mm upstream from trailing edge

With the fit the integral for the displacement thickness stated in (Eq.15) can be solved.

$$\delta^* \equiv \int_0^{y_1} \left(1 - \frac{\rho U}{\rho_\infty U_\infty}\right) dy \; (Eq. 15)$$

In this equation δ^* is the displacement thickness, ρ the density, U the velocity and y_1 states a position outside the boundary layer. ∞ states the flow conditions is free steam flow. Assumed is that the flow is incompressible, so (Eq.16) is left.

$$\delta^* = \int_0^{y_1} \left(1 - \frac{\rho U}{\rho_\infty U_\infty}\right) dy \; (Eq. 16)$$

To find the right value to compare the displacement thickness is determined at 1.3 mm from the trailing edge. The results are adjusted into Table 2. The trend of decreasing displacement thickness is faster than at the results of Brooks. The trend is fast because of the changing velocity profile. In the results of Brooks [2] this phenomena does not seem to happen. To get another reference in XFOIL calculations are made for the same conditions, this leads to a displacement thickness of 1.56 mm at 15 m/s and 0.78 mm at 35m/s. These results compare better with our results.

4.2.1.4 Strouhall number

There is tried to find a relation between the boundary thickness or displacement thickness and the Strouhall number stated in (Eq.17).

$$Str = \frac{f_p x}{U} (Eq.17)$$

In this case δ or δ^* is filled in for x. In Figure 25 the Strouhall number dependent on the boundary thickness, displacement thickness or a constant velocity is plotted against the velocity. Apart from the value at 15 m/s the trend is decreasing if the Strouhall number is scaled with the boundary- or displacement thickness. When there is scaled with a constant value the Strouhall number stays more constant. So scaling with the boundary thickness or displacement thickness is not advised.

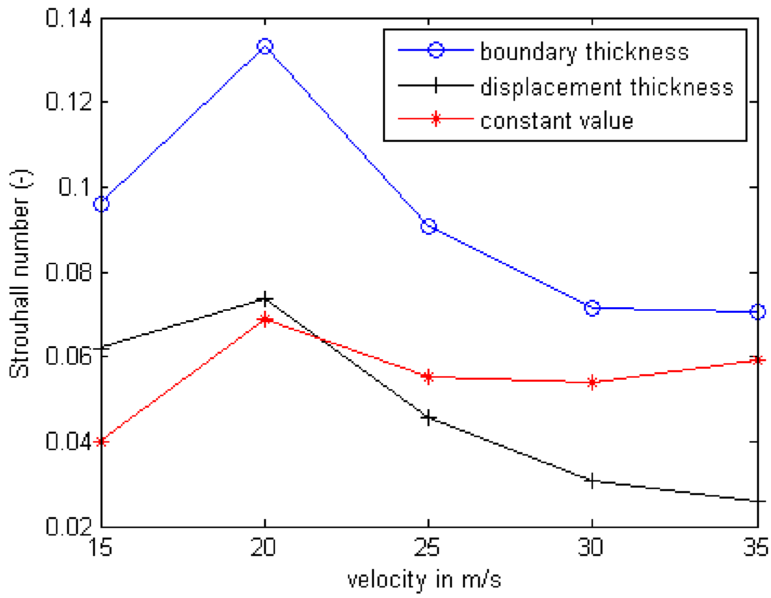

Figure 25 Strouhall number dependent on the boundary thickness, displacement thickness or a constant velocity plotted against the velocity

4.2.2 Power spectral density

In the acoustic measurement results different phenomena were hypothetically found to take place, to find out which phenomena take place at which angle of attack and velocity, in DaVis power spectrum density calculations are made.

In Figure 26 an example is shown of the results. In this case the origin of the noise is found at the pressure surface. In Table 3 is set out where the noise is created, separating laminar boundary shedding on the suction and pressure surface, and bluntness trailing edge vortex shedding. These results are based on the power spectral density graphs.

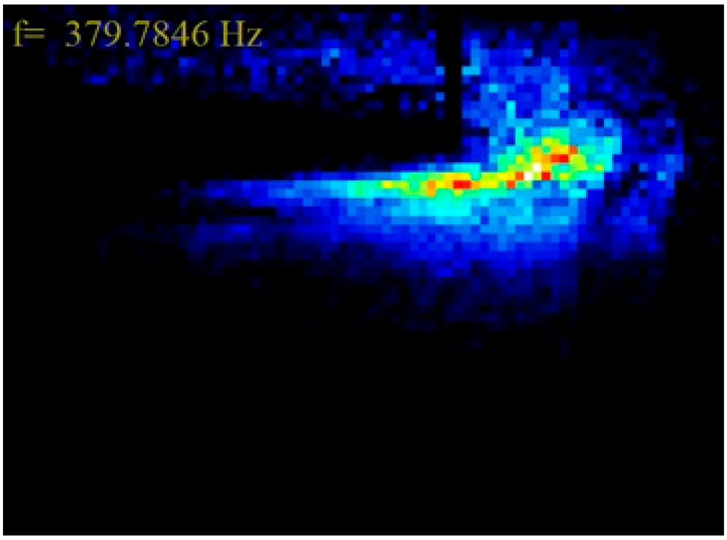

Figure 26 Power spectrum at an angle of attack of 2 degrees, a velocity of 25 m/s and four times the shown frequency

Table 3 Description where the sound is generated, in this table PS stands for pressure surface, SS means suction surface and B is noise generating because of bluntness trailing edge effects. N states that no noise effects are found

α / U	2°	4°	6°
15 m/s	SS	B	B
20 m/s	PS+SS	B	B
25 m/s	PS	B	N
30 m/s	PS	PS+B	N
35 m/s	PS+B	PS+B	N

An interesting result is that the tonal noise at 15 m/s and 20 m/s at an angle of attack of two degrees is influenced by the flow over the suction surface. Referring to Figure 11 the peak frequencies for these condition did not match with the scaling rules obtained for the other results. This is the reason for the deviations.

It is found that trailing edge bluntness vortex shedding is working together with laminar boundary layer vortex shedding. In the acoustic measurement the same transition was found as shown in Figure 16 and Figure 17. So, at this point the PIV measurements confirm the hypothetically found phenomena of the acoustic measurements.

4.2.2.1 Position based PSD

Next, power spectral density plots at different positions around the airfoil are made in the observed frequency range (till 1000 Hz). The measurements at 6.5 mm upstream from the trailing edge and 1 mm above the profile are taken. Peak frequencies appear in all the plots. The only peak obtained in the acoustic measurements in this frequency domain was at 15 m/s and an angle of attack of two degrees. This peak is found to be exactly on the same place as during the PIV measurements, Figure 27 shows that the peak is originated on the suction surface.

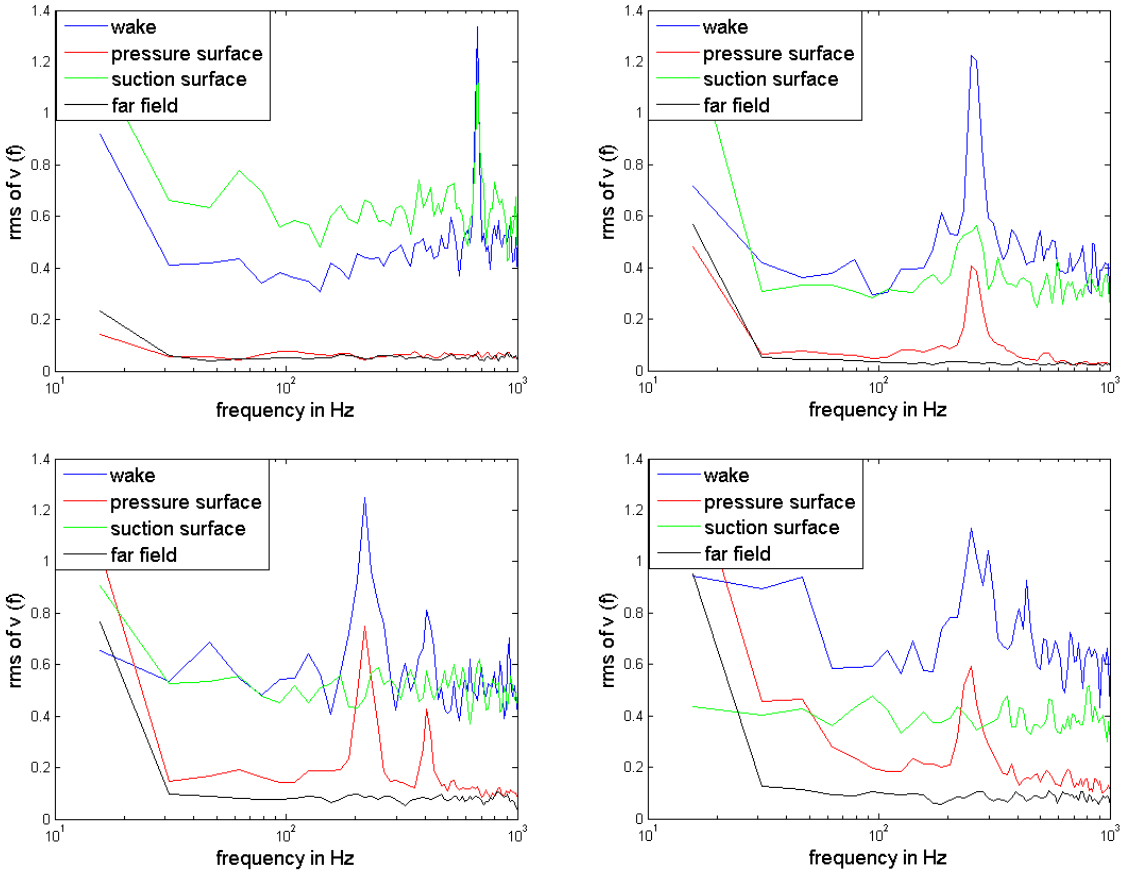

Figure 27 Root mean square of the velocity in y-direction in frequency domain in the situations of an angle of attack of 2 degrees and velocities of 15, 20, 25 and 35 m/s

Remarkable is the peak around 200-300 Hz that appears in the graphs with the other velocities in Figure 27. This peak was not found in acoustic measurements. Since the peaks at 200-300 Hz seem strange, there is checked if aliasing occurs. With a Nyquist frequency of 1000 Hz, a peak at 1700 to 1800 Hz could be represented. These frequencies compare well with the acoustic results. To be sure of these results in Figure 28 the velocity in y-direction around the trailing edge at one time step for an angle of attack of two degrees and a velocity of 30 m/s is represented. It shows a distance of one wave length of 8.5 mm. For the velocity of a vortex half U_∞ can be taken, resulting in a peak frequency of 1765 Hz. This compares well with the acoustic results and shows that the results are effected by aliasing.

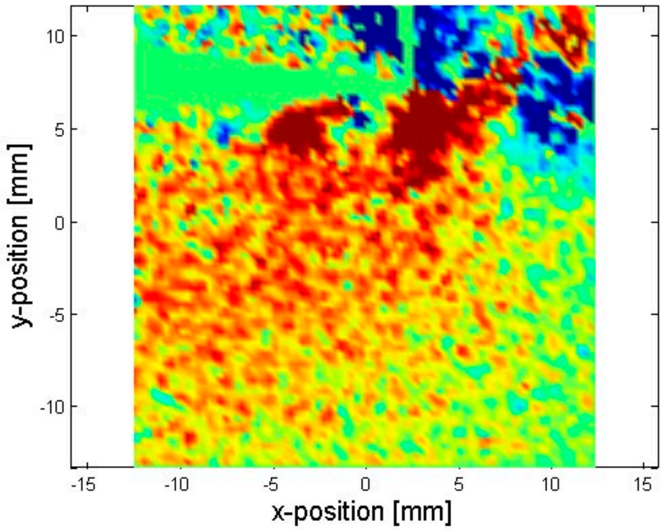

Figure 28 Representation of the flow velocity in y-direction around the trailing edge at one time step for an angle of attack of two degrees and a velocity of 30 m/s

4.2.2.2 Build-up of vortex strength

In this paragraph there is looked at the root mean square peak at conditions with just laminar boundary vortex shedding. As an example the root mean square of v in frequency domain at 30 m/s at pressure surface of the airfoil is taken, as shown in Figure 29. The measurements at 1 mm above the profile are taken. It is visible that the vortex in gaining strength while rolling over the airfoil.

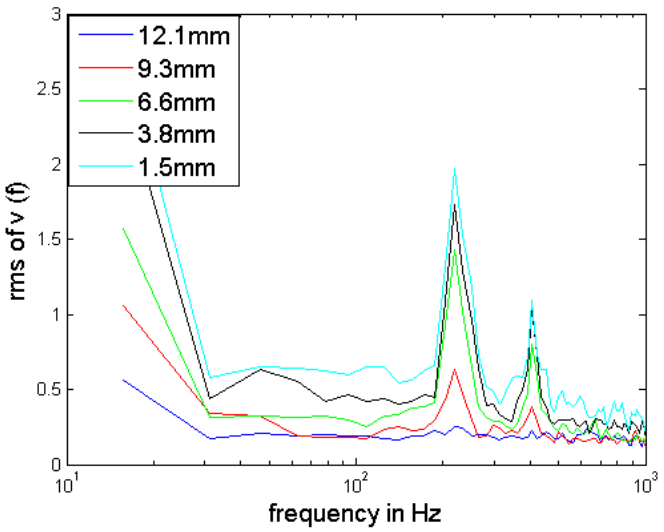

Figure 29 Rms at 35 m/s at pressure side of the airfoil

5 Conclusions & recommendations

5.1 Conclusions

This test report describes tonal noise generation by an NACA0012 airfoil at low to moderate Reynolds numbers. Intense narrow band tones have been found and both laminar boundary layer- and trailing edge bluntness vortex shedding noise was found for velocities of 15 m/s to 35 m/s. From 15 m/s till 27.5 m/s the phenomena worked separately, at higher speeds they start to collaborate. A linear scaling of the peak frequencies with the velocity is found and the condition at which tonal noise is observed is smaller than expected from literature. When the two phenomena work together the frequency of these peaks is repeatable, but the magnitude differs, resulting in a different maximum peak at a different measurement.

The goal in this report was to provide insight into the acoustic process by PIV measurements. It can be concluded that more insight into different aspects of tonal noise generated is given, since the PIV measurements gave inside in the deviations of the linear fit. At lower velocities it showed that the noise was (partly) created by the flow on the suction surface, and at higher velocities laminar boundary layer- and trailing edge bluntness vortex shedding work together. In this case a change in the velocity boundary layer profile is visible along the profile.

5.2 Recommendations

The results in a positive angle were different from the result in the same angle in negative direction. A PIV measurement at zero degrees of attack could give some more insight in these aspects. Further it can be advised to look well at the measurement frequency of the PIV system. Since a low frame rate is used, it was hard to obtain all tones in the PIV measurements.

6 References

[1] Paterson, R.W., Vogt, R., Fink, M.R. and Munch, C. L.: Vortex Noise of Isolated Airfoils, J.Aircraft, 10(1973, pp. 296-302)

[2] Brooks, T., Pope, D. and Marcolini, M.: "Airfoil Self-Noise and Prediction", NASA Reference Publication 1218, 1989

[3] Lowson, M.V., Fiddes, S.P., Nash, E.C.: Laminar Boundary Layer Aeroacoustic Instabilities, paper presented at 32nd Aerospace Sciences meeting & Exhibition, 1994

[4] Nash, E.C.,Lowson, M. V. and McAlpine, A.: Boundary Layer Instability Noise on Airfoils, J.Fluid Mech., 382(1999), pp.27-61.

[5] Anderson, John D., Jr.: "Fundamentals of Aerodynamics", 5th ed., McGraw-Hill Book Company, New York, 2011.